J Ther Eng, Vol. 11, No. 5, pp. 1420−1438, September, 2025

Journal of Thermal Engineering
Web page info: https://jten.yildiz.edu.tr
DOI: 10.14744/thermal.0000984

Research Article

Advanced thermal management in aircraft lithium-ion battery packs: optimization of heat dissipation using heat spreaders and phase change materials

Srinivas MALLIMOGGALA[1,*], K Rama DEVI[1]

[1]*Department of Electronics and Communication Engineering, JNTU College of Engineering Kakinada, A.P, India*

ARTICLE INFO

Article history
Received: 28 August 2024
Accepted: 10 December 2024

Keywords:
Aluminum Heat Spreaders; Battery Safety; Cooling Strategies, COMSOL Multiphysics; Heat Dissipation; Lithium-Ion Batteries; Thermal Management

ABSTRACT

Lithium-ion battery packs are essential in aviation, particularly for aircraft like the Cessna, Cirrus, and Piper models usually with 24V, and 16Ah to 35Ah capacities, depending on the specific model and avionics package installed, due to their high energy density and weight efficiency, which are critical for optimizing performance and fuel economy. This paper makes an exploration when it comes to spreading the heat from Auxiliary Power Unit (APU) battery packs with various cooling methods. This study addresses thermal management challenges, including the risk of thermal runaway, which can jeopardize safety challenges by optimizing heat dissipation in a 7s4p battery pack used in these aircraft, employing cooling techniques such as air cooling, phase change materials (PCMs), and aluminum-based heat spreaders (Al 3003-H18 and Al 6063-T83) to meet typical aviation requirements for reliability and efficiency. The simulations proved by COMSOL Multiphysics® pointed out that the aluminum variants especially the Al 3003-H18 significantly reduced peak temperatures (64.27 °C) compared to air cooling (82.36°C) at 8C, thus offered best thermal regime capability and managed the peak temperature as well as the voltage across the different rates of discharged. Pearson's correlation coefficient analysis also showed positive higher order linear regression between aluminum-based models highlighting their efficiency in dealing with the heat generation or thermal runaway. This work extends existing literature by applying aluminum heat spreaders for aviation-specific applications, offering new insights into the relationship between thermal properties and cooling strategies under high discharge conditions, thereby enhancing both safety and battery longevity in critical aviation operations.

Cite this article as: Mallimoggala S, Devi KR. Advanced thermal management in aircraft lithium-ion battery packs: optimization of heat dissipation using heat spreaders and phase change materials. J Ther Eng 2025;11(5):1420−1438.

***Corresponding author.**
*E-mail address: mallimoggla@gmail.com

This paper was recommended for publication in revised form by Editor-in-Chief Ahmet Selim Dalkilic

INTRODUCTION

Lithium-ion (Li-ion) batteries are highly sought after in aviation because of their high energy density, low weight, and versatility in terms of powering various aircraft equipment. They have proved to be more efficient and performance in comparison to the earlier used Nickel-Cadmium (Ni-Cd) batteries. The transition began markedly with Boeing 787 that has Li-ion battery for voltage regulation, starting the engine, and for other electrical operations. These batteries have some benefits; however, they are associated with thermal hazards of thermal runaway, and as a result demand effective Battery Thermal Management System (BTMS) to track conditions and failures [1].

Battery safety is crucial in preventing thermal runaway, a dangerous reaction that can lead to fires or explosions, especially in lithium-ion batteries. Such that an efficient thermal management is essential to control heat generation and mitigate the risks of overheating, ensuring safe operation in electric vehicles and other high-demand applications. Addressing such thermal runaway conditions is vital to protect users, improve battery reliability, and support the widespread adoption of lithium-ion technology. In dynamics of aviation, the utility of the BTMS rests upon on reliability aspects that must include safety, functions, standards, and technology. To lower fire hazards, at the same time have gross batteries for electric systems, which cuts down the usage of hydraulic or pneumatic systems. Public trust and operational approval in the industry can only be won when compliance with regulations is achieved [2].

Despite the future Boeing 777 coming up with safety issues of lithium-ion battery, the FAA came up with special conditions in 2013 [3,4], while the GA aircrafts like Cessna, Cirrus and Piper among others, utilize lead-acid batteries that are sealed with 24 volts and 16 Ah with battery models like Gill 7242-16 LT and Gill 7243-16 LT. These battery packs are non-noticeable, rugged and maintenance free and such are ideal to be used in short range aircraft [5,6].

The COMSOL Multiphysics® Reference Manual [7] is a comprehensive guide for engineers and researchers, providing detailed instructions on setting up simulations, applying boundary conditions, and solving complex multi-physics problems. The COMSOL Multiphysics® Battery Design Module is a guide for designing and battery modeling.

Liu et al. [8] emphasize the need for advanced thermal management of lithium-ion batteries in extreme conditions like high temperatures, fast charging, and preventing thermal runaway in EVs. The study explores external heat transfer systems and internal smart battery innovations with embedded sensors. However, it lacks practical analysis on integrating these external and internal systems, leaving a gap in understanding their real-world compatibility and effectiveness.

Figueiras et al. [9] explores hybrid-electric propulsion systems for regional aircraft in the FutPrInt50 project, focusing on three powertrain architectures: series, parallel, and turboelectric. Using computational and experimental data, parametric studies evaluate the effects of battery parameters and hybridization factors on performance. A thermal management system and multi-objective optimization aim to minimize mass and emissions. While the study offers performance insights, it lacks details on real-world scalability, experimental data sources, and practical feasibility for broader commercial applications.

Coutinho et al. [10] explores thermal management systems (TMS) for hybrid-electric aircraft propulsion to manage waste heat and reduce emissions. Five TMS architectures are modeled using Matlab/Simulink, comparing their cooling performance and impact on flight. Results does not show a single architecture is ideal, indicating the need for further development.

Capron et al. [11] gives a paper that employs COMSOL Multiphysics® and MATLAB® modeling to analyze the temperature distribution of battery packs. They derive two 2D models with homogenized thermal properties and other model with cell layer properties in detail to have enhanced thermal specifications. Shetty et al. [12] investigates the use of mini-channel cooling plates with a streamline configuration for thermal management of Li-ion batteries in electric vehicles. Computational analysis of five plates with varying channel numbers (3-7) at a coolant flow rate of 0.002 kg/s showed a 7.8% reduction in maximum cell temperature for the 7-channel design. Temperature uniformity also improved, suggesting this design effectively maintains battery temperatures within a safe range and could enhance future battery thermal management systems.

Zhu et al. [13] presents an improved simulation method for small-size, fast-activation thermal batteries using the COMSOL platform. A two-dimensional axisymmetric model was developed to simulate temperature changes and electrolyte melting under high-temperature conditions (50°C). The results show that additional heating flakes and improved insulation reduce heat loss, with most melting heat flowing from the negative side. The activation time of the thermal battery was calculated to be 91.2ms, with an error margin within 10% compared to experimental results, demonstrating the model's high accuracy and broader applicability for thermal battery simulations.

Zhao, Chen, and He [14] focus on the thermal management of nickel-cobalt lithium manganate (NCM) batteries for electric vehicles, using COMSOL to simulate five liquid-cooled temperature control models. A performance evaluation system based on the analytic network process (ANP) and system dynamics (SD) ranks Models 1 and 5 as the most effective. However, the study lacks real-world testing and validation, leaving a gap in understanding how these models would perform in practical conditions.

A thermal model for lithium-ion battery cells and packs is developed for COMSOL Multiphysics® by Dunning et al. [15] which modeled a battery cell, incorporating factors like electrode thickness and particle size. A 5C discharge simulation showed a 14°C temperature rise for a single cell,

validated against experimental data. When applied to a battery pack, the temperature increase was 19.6°C, with a 9% error margin. While effective for preliminary design, the study lacks real-world validation and practical insights for large-scale applications.

Sun et al. [16] assesses a battery thermal management system (BTMS) with phase change materials (PCMs) and liquid cooling. It discovers that incorporation of the PCM with liquid cooling leads to reduction of the maximum temperature and enhancement of the thermal uniformity with 10% mass fraction expanded graphite in paraffin wax PCM.

V. K. Satheesh et al. [17] proposes a converging tapered airflow duct to enhance temperature uniformity and reduce peak temperatures. Using computational fluid dynamics validated by experimental data, the tapered design improved heat dissipation and reduced peak temperature rise by 20% and temperature variation by 19%. However, the study lacks insights into practical integration and long-term durability of the proposed duct in real-world electric vehicle applications.

P. R. Gharde and S. N. Havaldar, [18] investigates a floating capsule thermal energy storage system (TESS) using beeswax and paraffin as phase change materials (PCMs) to improve heat storage capacity. The system features spherical capsules filled with beeswax within a paraffin-filled cylindrical shell, with heat transfer fluid flowing through hexagonal tubes. A mathematical model predicts a 21.5% increase in storage capacity with a 70–30% beeswax-paraffin mix. Charging and discharging times were estimated at 2.6 and 3.2 hours, respectively. However, the study lacks real-world testing, and the long-term stability of the PCMs is not discussed.

S. Gungor et al. [19] highlights the critical role of thermal management strategies for lithium-ion (Li-ion) batteries, especially as transportation and electricity generation shift towards renewable sources. And compares various thermal management strategies based on battery geometry, coolant type, and heat transfer methods, but lacks detailed analysis on post-lithium batteries and real-world scalability of these strategies in the EV industry.

B. Palmieri et al. [20] used high thermally conductive materials, particularly graphite nanoplatelet films, is being explored to enhance battery performance and safety by improving heat dissipation. This study employs a numerical model using the finite element method in COMSOL to predict heat generation during charging and discharging cycles. The findings indicate that integrating thermally conductive materials can protect neighboring cells from heat propagation, helping to maintain uniform temperature and delay thermal runaway in battery modules.

The main objective of this paper is to review and implement an enhanced thermal system in a 24V 16Ah lithium-ion battery pack used in aircraft application; the APU battery packs. Specifically, these battery packs are essential in ensuring constant power to several aircraft systems, and the efficiency and effectiveness of the systems are determined by the battery packs' performance. Since lithium-ion batteries are define by high thermal risks such as thermal runaway where the battery produces high heat and, in some cases, cause fires, heat management is crucial.

Based on the above objective, the study incorporates an extensive Simulation technique by applying COMSOL Multiphysics® to study thermal characteristics of a 7s4p battery layout. Consideration is given to several cooling methods based on air circulation as well as PCMs and various heat spreaders made of aluminum. Thus, the goals of the study, which focus on the comparison of the thermal characteristics of these materials and cooling methods, are to determine how heat can be shed and battery temperature regulated under different discharge rates.

In addition, the present research focuses on the identification of various cooling options and their effects on the battery temperature and voltage on the strength. This involves studying the aluminum variants like Al 3003-H18 against other materials- in matters to do with sustaining lower values of maximum peak temperature and constant value of voltage.

This research study is poised to contribute its findings towards improving the thermal management systems for lithium-ion batteries in application in aviation hence improving on their safety and durability. Lastly, it is the hope of this paper to present useful information and recommendation to the engineers and researchers involved in the thermal management of battery in aviation while contributing to the general objective of enhancing the application of lithium-ion batteries in aircraft while providing operational safety and efficiency.

MODELING AND METHODOLOGY

This battery configuration and capacity of A 24V, 16Ah lithium-ion battery pack has a lot of advantages for GA aircrafts such as Cessna, Cirrus, and Piper. It has a longer cycle life, require less maintenance, increases starter power, and the Battery Management system. These batteries can interface directly with the new age avionics and electrical systems and deliver stable voltage as well as sufficient current. Besides, they are safe for environment as they do not include toxic component, namely lead.

In the thermal model of the battery pack, the primary heat source is the heat generated during the battery's discharge process. This heat generation is a result of the internal resistance and discharge rate (C-rate) of the battery cells. When modeling large battery packs, detailed geometrical and chemical information about individual battery cells may be impractical due to computational constraints, leading to the use of simpler zero-dimensional models [21]. These models, like equivalent circuits or lumped battery models, aggregate the complex interactions of ions and voltages into simplified representations, enabling efficient analysis of cell-to-cell current distribution within the pack.

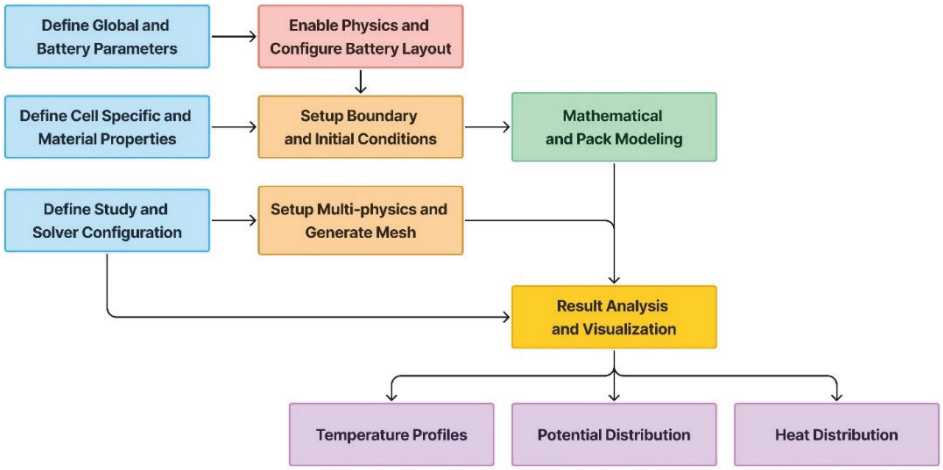

Figure 1. Flowchart for battery pack simulation process in COMSOL.

The modeling and simulation are performed by the help of multipurpose software 'COMSOL Multiphysics®.

Figure 1 depicts the flowchart which indicates a detailed methodological approach to the simulation of battery systems based on the global parameters and the properties of the materials used. This includes development in physical architecture layout of the battery, the imposition of constraints on the problem formulation by defining the boundary conditions, inputting of solver settings, generation of the mesh to discretize the problem, mathematical modeling of the battery pack and interpretation of results as concerns the distribution of temperature of the battery bundles, the distribution of the potential across the battery pack and the distribution of heat generation for purposes of optimization.

Geometry and Battery Parameters

Another way that the researchers present the parameters is a table 1 with a detailed lookup of parameters that has been divided into Battery Pack Metrics, Physical Dimensions, Cooling Plate Dimensions, Layout Configuration, Electrical Parameters, Activation Energies, Thermal Properties, and Initial Conditions. This data is useful for creating and prototyping battery packs with performance parameters assessed under various system operational situations and system designs.

Battery Pack Metrics, Physical Dimensions, and Cooling Plates Dimensions can be seen as fundamental components of a battery pack, that explain what the battery pack is capable of and what it cannot do. They include nominal voltage, full charge voltage, capacity, and the current at the different discharge rates. Some of the non-electrical parameters, which include battery diameter, height, and sizes of the connectors, are critical in developing geometrical models in the simulation process. Cooling Plates Dimensions contain detailed information on cooling plates' dimensions for distinct models (B, C, D), which means that simulations take into consideration the real space occupied and x-coordinate for evaluating their performance in heat dissipation.

Boundary and Initial Conditions

Table 1 also can be associated with the exterior and inside conditions of the battery pack, for instance, thermal properties, electrical parameters, as well as the outer/inner limits of the battery pack. The Thermal Properties part of the table contains such parameters as "thermal conductivity in-plane "battery density and "battery heat capacity," which define thermal interaction with the battery cells and between them. heat transfer coefficient, defines heat exchange with the environment and affects the thermal behavior of the battery pack.

Electrical Parameters assist in simulating the electrochemical behavior in battery packs making constant voltage and specific resistance, while the Activation Energies section assists in the determination of electrode materials. These conditions mimic the functioning of the battery pack when it is in the state of charging and discharging and under varying electrical loads. Geometric sizes of battery such as the diameter, the radius, and the height of battery and the cooling plate size which provide the overall spatial condition for modeling the battery pack since they determine space and mechanical interfaces of the system is provided in table 1.

"E_OCP," which stands for Open Circuit Potential, is the voltage of batteries when the currents are not flowing through it and it is recharging or discharging; its relation with the degree of charge is very important to monitor the behavior of batteries; therefore, E_OCP plays the role of a significant input for simulators that are used for assessing the battery life. Thus, "dEdT", the Derivative of Voltage with Respect to Temperature is important to control battery thermal state and designing proper cooling in COMSOL effected environments where temperature varies frequently. Therefore, assist in designing batteries that are efficient as

Table 1. Battery pack parameters and configurations for modeling

Category	Name	Value	Description
Battery pack Metrics	Simulated time	720	Model Simulation time period (s)
	Nominal voltage	24.6	Nominal Voltage of Battery Pack (V)
	Full Charge voltage	29.4	Full Charge Voltage of Battery Pack (V)
	Nominal battery capacity	16	Nominal Battery Pack Capacity (Ah)
	0.5C discharge rate	8	Discharge current at 0.5C (A)
	1C discharge rate	16	Discharge current at 1C (A)
	2C discharge rate	32	Discharge current at 2C (A)
	4C discharge rate	64	Discharge current at 4C (A)
	6C discharge rate	96	Discharge current at 6C (A)
	8C discharge rate	128	Discharge current at 8C (A)
Physical Dimensions	Battery diameter	18	Battery diameter (mm)
	Battery radius	9	Battery radius (mm)
	Battery height	65	Battery height (mm)
	Terminal height	1	Terminal height (mm)
	Terminal radius	3	Terminal radius (mm)
	Serial connector width	2	Serial connector width (mm)
	Serial connector height	1	Serial connector height (mm)
	Parallel connector height	0.5	Parallel connector height (mm)
	Parallel connector Width	1	Parallel connector width (mm)
Cooling Plates dimensions (Width × depth × height)	Series plate dimension Model-B	9 × 99 × 65	Series Plate dimension Model B (mm)
	Parallel plate dimension for model-B	180 × 9 × 65	Parallel Plate dimension for Model B (mm)
	Plate dimension for model C	9 × 72 × 65	Plate dimension for Model C (mm)
	Plate dimension for model D	126 × 9 × 65	Plate dimension for Model D (mm)
	Total number of batteries	28	Total Number of cells in the battery pack
Layout Configuration	Number of batteries - X	7	Number of batteries in x-direction
	Number of batteries - Y	4	Number of batteries in y-direction
	Number of plates - X	6	Number of plates in x-direction
	Number of plates - Y	3	Number of plates in y-direction
Electrical Parameters	Battery cell capacity	4	Battery cell capacity (Ah)
	Current-1C	4	1C current (A)
	C-rate	0.5, 1, 2, 4, 6, 8	C rates indicating the rate of charge/discharge (C)
Activation Energies	Activation energy for eta1C	24000	Activation energy (J/mol) associated with resistive property
	Activation energy for J0	−59000	Activation energy (J/mol) relates to the current density
	Activation energy for Tau	24000	Activation energy (J/mol) with a time constant (τ)
Thermal Properties	Thermal conductivity in-plane	30	Thermal conductivity in-plane (W/m·K)
	Thermal conductivity cross-plane	1	Thermal conductivity cross-plane (W/m·K)
	Battery density	2000	Battery density (kg/m^3)
	Battery heat capacity	1400	Battery heat capacity (J/kg·K)
	Heat transfer coefficient	30	Heat transfer coefficient ($W/m^2 \cdot K$)
Initial Conditions	Reference temperature	293.15	Reference temperature (K)
	Reference temperature J0	0.85	J0 at reference temperature (A/m^2)
	Reference tau time	1000	tau at reference time (s)
	Reference voltage eta_1C	0.0045	eta_1C at reference voltage (V)
	Int-ex temperature	293.15	Initial/external temperature (K)

well as safe by giving a holistic and detailed prospect of how they will behave in different electrical loads and various thermal conditions.

When it comes to the 7s4p battery pack configuration, for probe selection where cells are 1-28, cell temperature and cell potential are to be monitored. This selection includes all the cells in the battery pack making sure that thermal and electrical characterization of the array is completely captured. It is important to track these parameters if one intends to know how each cell is behaving in different operations to ensure the required performance, safety and durability of the battery system is achieved.

Layout Configuration and Material Properties

This paper presents four individual models of a 7s4p battery pack structure with different positions of the cells and cooling plates for thermal management schemata, as shown in Figure 2(a). Heat spreaders are another pair of plates with configurations of series, parallel, and grids connected to the batteries' directions. The construction parameter that has been used in the modeling is described in the following table 1.

Model A is a straight or inline pack that consist of twenty-eight individual cells labelled 1 through to 28 and for this model there are no cooling plates employed. In Model B the grid format which is compact, has more rigid rows and columns of the cells thus enhancing the uniformity of cooling. Enduring cooling plates which were positioned in PP1 to PP3 as well as SP1 to SP6, which increases the utilization and efficiency by creating a direct heat dissipation channel from cells to the cooling plates.

Model C and Model D in addition to the above model for heat distribution, it alters the mode of the cells in series and parallel for redundancy. Coupling plates SP1 to SP6 and pre-plates PP1 to PP3 are disposed between the plates like as shown in Model B. In addition, different materials are utilization to perform testing for Model B to establish the most efficient type of passive cooling system.

The characteristics of the free tetrahedral mesh used in simulations for proposed four different battery pack models (A, B, C, D) are shown in the Table 2. This data is instrumental in assessing the quality and the level of detail of the mesh required for FEM simulations which are very important for computational modelling of physical processes in the battery packs.

This figure 2(b) illustrates the temperature-dependent behavior of key material properties in a battery pack system, along with a schematic of the battery's physical layout. The graphs show that as temperature increases, the dynamic viscosity (η(T)) and specific heat capacity (Cp(T)) rise, while the density (ρ(T)) decreases. Additionally, the thermal conductivity (k(T)) and speed of sound (cs(T)) both increase with temperature. These trends are important for understanding the thermal performance and material stability of the battery pack during operation.

Some of the types of meshes that are used include vertices, tetrahedra, triangles, edge elements, vertex elements, minimum element quality, average element quality, element volume ratio, mesh volume, space dimension, domains, boundaries, edges, and vertices. Quality of the mesh impacts simulations and the lower and average elements impact it bearing stability and accuracy. The number of nodes must be equal to the size of the modelled object, the size dimension should be set to 3. Another factor that helps create a mesh with better detail is also counting of the number of domains, boundary, edges, and vertices.

It is helpful when it comes to creating quality mesh in simulations to pick up all the necessary physical events. Such characteristics as minimum quality and average quality cause shifts in the range of results' stability and reliability. The implementation of the well-constructed mesh allows one to predict and analyze the battery pack's physical behaviors more efficiently. This table offers a specific description of mesh characteristics in each model, so that the researchers can judge the mesh for the capability of the analysis of the complex behavior and its adequacy in different configurations of the model.

Figure 3, also gives a clear and comprehensive comparison of four Battery pack models (A, B, C, D) that shows the design aspects which could use for further examination in simulation for purpose of optimization, the figure offers a broad perception of the structural and systems and features of the Battery pack models for the purpose of analysis.

For each model of the housing, different designs are incorporated to safeguard the inner most parts of the battery packs, including the mechanical and external aspects. Mesh design visualizations are essential for the simulation

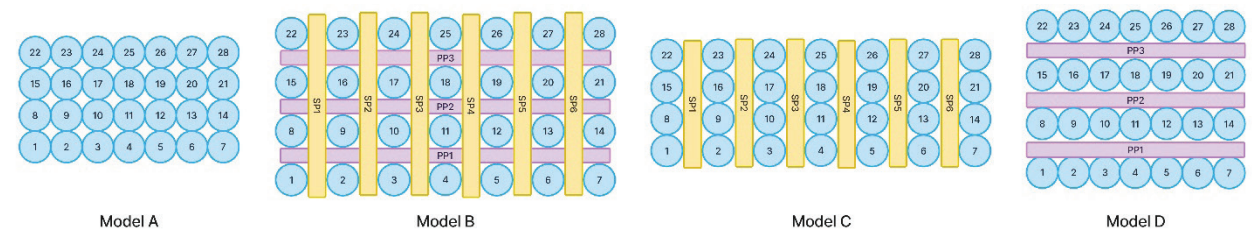

Figure 2(a). Schematic Layouts of Battery Pack Configurations: Models A, B, C, and D.

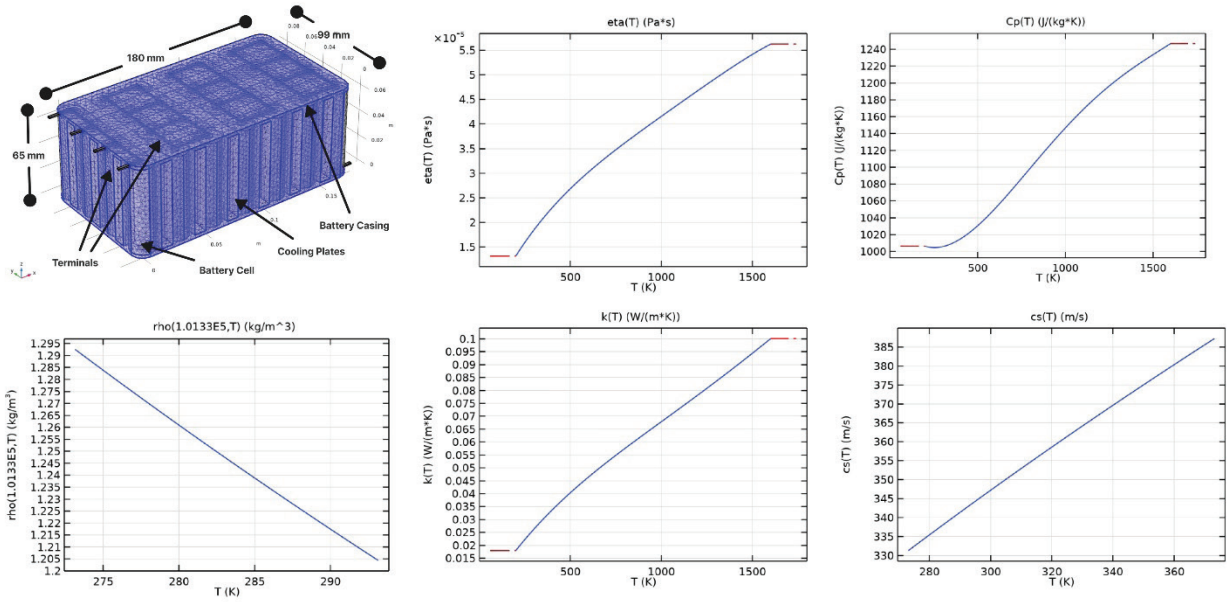

Figure 3(b). Thermal and Material Properties of Battery Pack Components as a Function of Temperature.

Table 2. Comparison of mesh characteristics and quality metrics across models A, B, C, and D

Type	Parameter	Model A	Model B	Model C	Model D
Free Tetrahedral mesh	**Mesh vertices**	52554	54316	44698	69895
	Tetrahedra	291782	304479	249897	392250
	Triangles	68149	75108	62833	90140
	Edge elements	8276	12021	9038	10289
	Vertex elements	1386	1704	1482	1452
	Number of elements	291782	304479	249897	392250
	Minimum element quality	0.04949	0.01485	0.0203	0.01798
	Average element quality	0.5787	0.5617	0.5548	0.5757
	Element volume ratio	5.75E-04	3.40E-04	3.55E-04	5.34E-04
	Mesh volume (m^3)	6.339E-4	0.001242	9.06E-4	8.72E-4
Geometry	**Space dimension**	3	3	3	3
	Number of domains	223	224	229	226
	Number of boundaries	1417	1750	1501	1477
	Number of edges	2068	3328	2800	2749
	Number of vertices	1386	1704	1482	1452
Battery Volumetrics	**Battery Cell Volume (m^3)**	1.65×10^{-5}	1.65×10^{-5}	1.65×10^{-5}	1.65×10^{-5}
	Battery Pack Volume (m^3)	4.62×10^{-5}	4.62×10^{-5}	4.62×10^{-5}	4.62×10^{-5}
	Total Volume of Cooling Plates (m^3)	-	6.63×10^{-4}	4.21×10^{-5}	7.37×10^{-5}

to be accurate, because they show computational grids that are used in finite element analysis.

As for terminals, they impact the electrical efficiency and performance; concerning active battery configurations, they define space, connectivity, and thermal properties. The cooling design is shown for each model, only for Model A, no integrated cooling system is present. Among the presented models, B, C, and D have cooling systems, which proves that they are designed for critical applications.

Table 3 depicts a list of materials and their thermal characteristics that exist in a 7s4p battery design. It lists the materials that should be avoided when constructing the battery terminals and Active battery as well as different cooling methods. Battery terminals and active battery components are said to be

Table 3. Material properties for plates used in battery pack models

Condition	Material	Heat capacity at constant pressure (J/kg·K)	Thermal conductivity (W/m·K)	Density (kg/m³)
Battery terminals	**Aluminum**	900	238	2700
Active battery	**lithium- ion**	1400	30	2000
Cooling model A	7s4p Straight configuration without cooling			
Cooling model B1	**Air**	1005	0.026	1.225
Cooling model B2	**Paraffin solid**	1850	0.4	861
Cooling model B3	**Paraffin liquid**	2384	0.15	778
Cooling model B4	**Aluminum**	900	238	2700
Cooling model B5	**Aluminum 6063-T83**	900	201	2700
Cooling model B6	**Aluminum 3003-H18**	893	155	2730
Cooling model C	**Aluminum in Series**	900	238	2700
Cooling model D	**Aluminum in Parallel**	900	238	2700

made of aluminum or lithium-ion and their heat and electrical conductivity, density, and heat capacity is given.

This table 3 also presents four cooling models: A Model A without any cooling plates. Model B utilization includes air, PCM (paraffin) as well as heat spreaders (aluminum and its alloys). And Model C and D, it employs the use of aluminum in series and parallel circuits separately. Thus, the specific objectives are the following: Assess the thermal conductivity and apparent heat capacity of air, paraffin, aluminum and aluminum alloys (6063-T83, 3003-H18) in various battery pack arrangements.

Multiphysics and Mathematical Model

Some basic equations that are frequently used while modeling the electrochemical as well as the thermal aspects of a battery cell includes Cell Voltage Equation represented by (1), The definition of 1C current represented by equation (2), applied current as represented by equation (3), Volume integral of voltage as represented by equation (4), Normalization condition as represented by equation (5). These equations define several coefficients related to electrical characteristics of battery cells, voltage, current and internal processes that are important in the battery cell simulation and creation of control algorithms in the battery management systems [20].

$$E_{cell} = E_{OCV}(SOC, T) + \eta_{IR} + \eta_{act} \quad (1)$$

$$I_{1C} = \frac{Q_{cell,0}}{3600(s)} \quad (2)$$

$$I_{cell} = I_{app} \quad (3)$$

$$V_{cell} = \int_{\Omega_{cell}} d_{vol}\Omega \quad (4)$$

$$d_{vol} = 1 \quad (5)$$

The thermal, electrochemical working in a battery cell, including the thermal aspect, heat production and the relation between both aspects. The Heat Equation with Internal Heat Generation: heat conduction in solids (6) and liquids (7) are important tool for describing thermal processes in battery and evaluating temperature fields. They include heat conduction, convective heat transfer, and internal heat generation and takes account of it (8).

$$\rho c_p \frac{\partial T}{\partial t} = \nabla \cdot (k\nabla T) + Q_h \quad (6)$$

$$\rho c_p \frac{\partial T}{\partial t} + \rho c_p u \cdot \nabla T = \nabla \cdot (k\nabla T) + Q_h \quad (7)$$

$$Q_h = \left(\eta_{IR} + \eta_{act} + T\frac{\partial E_{OCV}(SOC|_{X=1,T})}{\partial T}\right) I_{cell} + Q_{mix} \quad (8)$$

These equations provided describe various aspects of thermal dynamics within a battery system. The Mixing Heat Equation (9) calculates the heat generated from mixing processes within the battery. The Thermal Open-Circuit Voltage Equation (10) defines how the thermal effects alter the open-circuit voltage. The Thermal Conduction Equation (11) illustrates the relationship between thermal conductivity and heat transfer, where the heat flux is proportional to the temperature gradient within the material and the difference between the surface temperature and ambient temperature. Together, these equations provide a comprehensive framework for understanding thermal management in battery design [7].

$$Q_{mix} = \frac{3Q_{cell}}{\tau} \int_0^1 \left(\frac{\partial E_{OCV,therm}}{\partial SOC}\frac{\partial SOC}{\partial x}\frac{\partial SOC}{\partial x}\, x^2 dx\right) \quad (9)$$

$$E_{OCV,therm} = E_{OCV,ref}(SOC) - T_{ref}\frac{\partial E_{OCV}(SOC)}{\partial T} \quad (10)$$

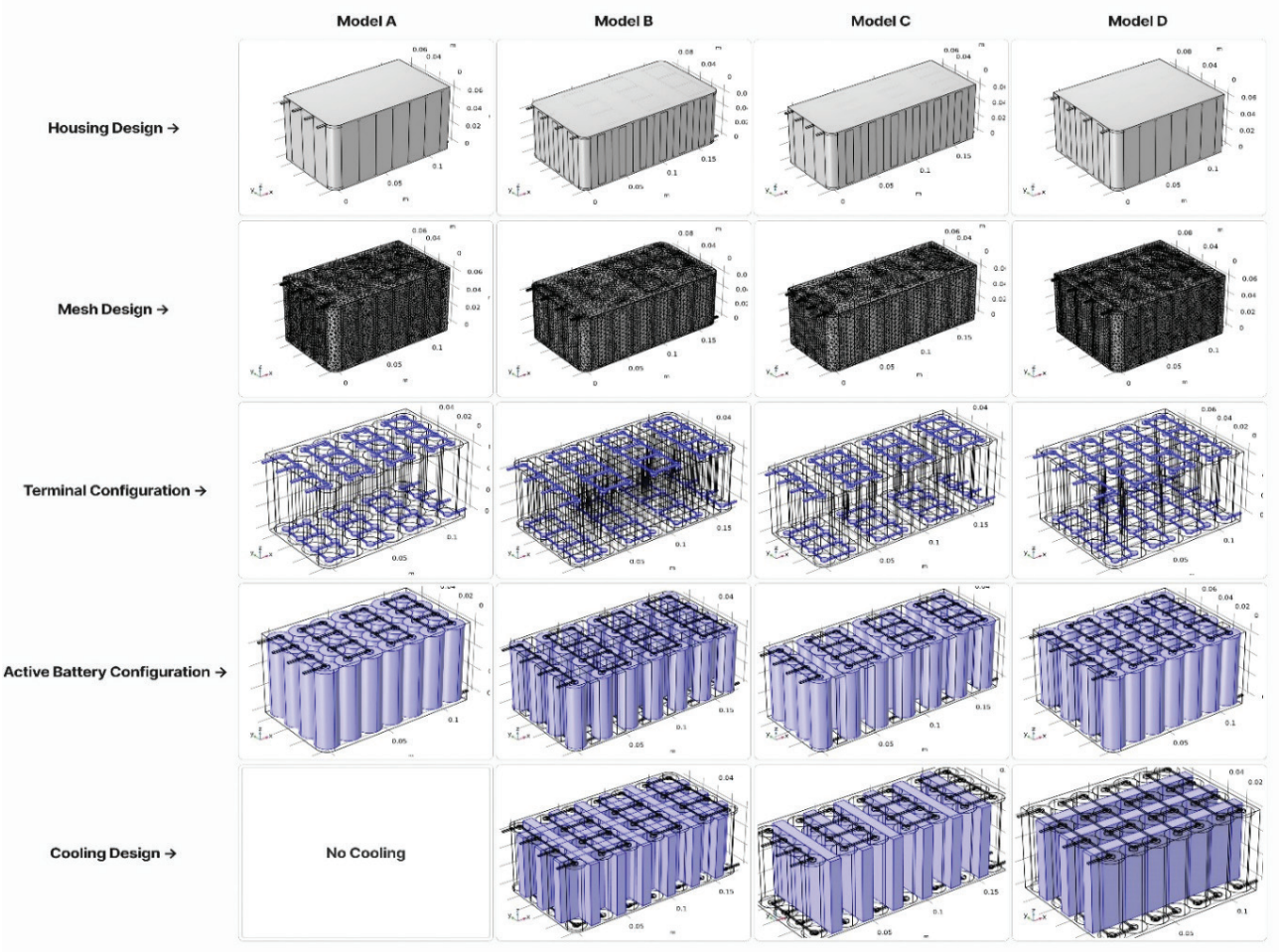

Figure 4. Comparison of Battery Pack Configurations and Cooling Designs.

$$-k_s \frac{\partial T}{\partial n} = h_{nat}(T_s - T_a) \tag{11}$$

These equations are critical for simulations of the battery thermal management and safety and can be used to optimize the design of the thermal systems, reduction of the risk of thermal runaway and setting up thermal safe limits. They also forecast temperatures and their effects on batteries with respect to their usage in different applications and life span [7,22]. Equations for heat transfer through boundaries: (12) equations for heat convection: (13) and for heat accumulation and specific heats (14).

$$q = -k\nabla T \tag{12}$$

$$q_{conv} = h(T_s - T_a) \tag{13}$$

$$\rho c_p \frac{\partial T}{\partial t} = \nabla \cdot (k\nabla T) + Q_h \tag{14}$$

To determine the thermal behavior of the battery pack during operation, theoretical calculations were performed based on the relevant input parameters provided in Table 1. These calculations consider the battery pack metrics, physical dimensions, cooling plate dimensions, layout configuration, electrical parameters, activation energies, thermal properties, and initial conditions. The heat generated within the battery pack due to internal resistance during discharge was calculated using Joule's law, as shown in Equation (15), Total Heat Capacity of the System (16), Temperature Rise of the System (17)

$$Q_b = N_{cell} \times I^2 \times R \times t \tag{15}$$

$$C_{total} = (m_{battery} \times c_{battery}) + (m_{aluminum} \times c_{aluminum}) \tag{16}$$

$$\Delta T = \frac{Q_b}{C_{total}} \tag{17}$$

$$T_T = T_0 + \Delta T \tag{18}$$

Where: N_{cell} is 28 (number of cells), I is the discharge current for each C-rate (as presented in Table 1), R is the internal resistance of the cells (0.005 Ω), t is the discharge

time (720 s), TT is total temperature, T0 is the initial temperature. For example, let us consider the M-B6 at a 0.5C discharge rate, the current is I = 2 A, C_{total} is the total heat capacity of the system, $m_{battery}$ and $m_{aluminum}$ is the mass of the battery and aluminum respectively, similarly $c_{battery}$ and $c_{aluminum}$ for specific heat capacity of battery and aluminum respectively. Therefore, the heat generated by the battery pack is:

$Q_b(0.5c) = 28 \times (2)2 \times 0.005 \times 720 = 403.2J.$

$$\Delta T = \frac{403.2}{2909.93} \approx 0.14°C$$

$$T_T = 20 + 0.14 = 20.14$$

For the 1C discharge rate (I = 4A):

$Q_b(1c) = 28 \times (4)2 \times 0.005 \times 720 = 1612.8J.$

$$\Delta T = \frac{1612.8}{2909.93} \approx 0.55°C$$

$$T_T = 20 + 0.55 = 20.55$$

Similarly, the other values can be calculated in the same process and get 22.22°C, 28.86°C, 39.95°C, 55.47°C for 2C, 4C, 6C, 8C respectively.

RESULTS AND DISCUSSION

The testing was conducted at an ambient temperature of 20°C with various discharge C-rates, of at 0.5C, 1C, 2C, 4C, 6C, and 8C, rate currents to perform a comprehensive analysis on the thermal conditions of the battery pack arrangements. The experimental results were meticulously analyzed to assess several critical aspects of Temperature Profiles and Voltage Profiles as presented in figures 4 and 5, Peak Temperatures Comparison presented in figure 6 thermal distribution also known as Heat Profile presented in figure 7 and at last the Correlation Matrix of Different Battery Pack Configurations presented in figure 8.

The distribution of thermal and electrical performance of different configurations is given in figures 4, 5 & 6 and table 4. Critical factors of battery performance have been analyzed for this paper and sensitivity analysis has been done to emphasize the best cooling strategies. From the following the models are represented as M-A (Model A), M-B1 (Model B1 (Air)), M-B2 (Model B2 (Paraffin Solid)), M-B3(Model B3(Paraffin Liquid)), M-B4 (Model B4(Aluminum)), M-B5 (Model B5(Al 6063-T83)), M-B6 (Model B6 (Al 3003-H18)), M-C (Model C (Aluminum in series)), M-D (Model D (Aluminum in parallel)).

Temperature Management and Temperature Profiles

Discharge rate has a great influence on the temperature regulation which is regarded as the key factor. Higher discharge rates cause the efficiency to be lower meaning that for all the configurations there is a greater temperature rise as seen in figure 4. The rate at which the technique cools the product is also an essential aspect. Comparing between the cooling methods with aluminum, this investigation reveals that M-B4 , M-B5, and M-B6 exhibit higher thermal control in the cooling system than the methods using M-B1, M-B2 and M-B3 air and PCM (paraffin).

From observing the figures 4, 5(a-c) and table 4 we can determine the cooling efficiency of each model. At 0.5C discharge rate for M-A, M-B1, M-B2, M-B3, M-B4, M-B5, M-B6, M-C, and M-D, the peak temperature raises from 20°C (initial temperature) to 21.64°C, 21.34°C, 20.99°C,

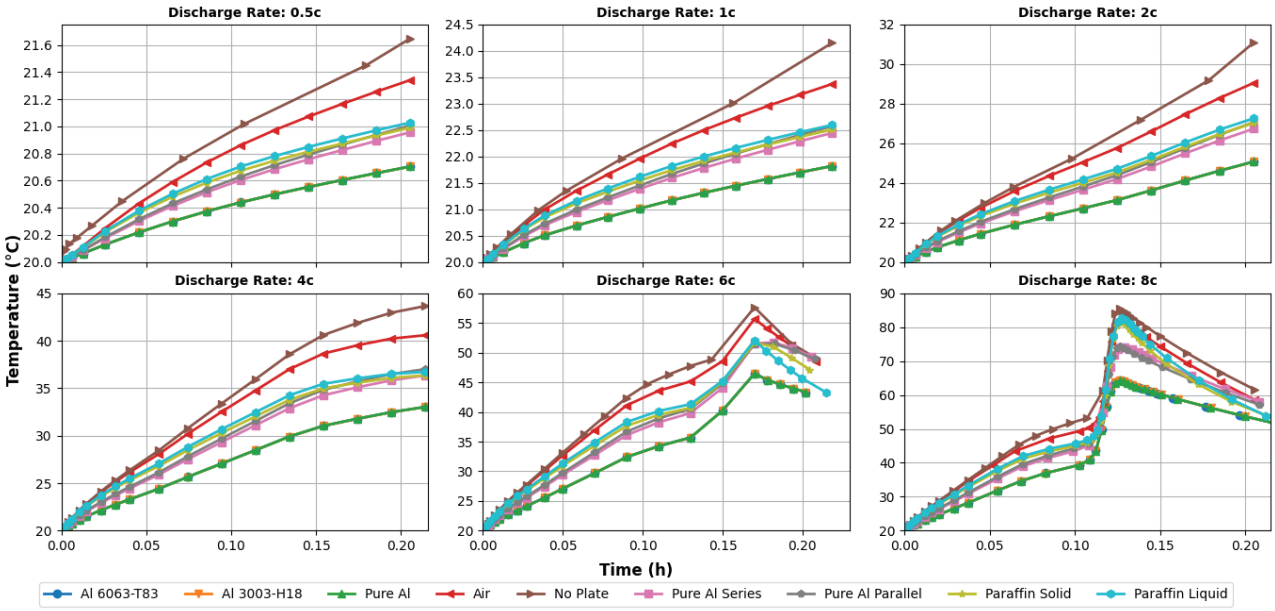

Figure 5. Temperature Profiles of Battery Pack Configurations Under Various Discharge Rates.

21.02°C, 20.7°C, 20.7°C, 20.7°C, 20.95°C, and 21°C respectively. Similarly, at 1C discharge rate, the peak temperature rises to 24.15°C, 23.37°C, 22.51°C, 22.59°C, 21.82°C, 21.82°C, 21.82°C, 22.44°C, and 22.57°C respectively. At 2C discharge rate, the peak temperature rises further to 31.08°C, 29.04°C, 27.02°C, 27.25°C, 25.07°C, 25.07°C, 25.06°C, 26.73°C, and 27.05°C. At 4C discharge rate, the peak temperatures increase significantly, reaching 43.64°C, 40.57°C, 36.35°C, 36.72°C, 33.02°C, 33.02°C, 33.01°C, 36.34°C, and 37.01°C respectively.

At 6C discharge rate, the peak temperatures rise to 57.6°C, 55.66°C, 51.62°C, 52.63°C, 46.45°C, 46.46°C, 46.45°C, 51.73°C, and 51.49°C at 0.2 hours during the 6C discharge, the temperatures stabilize at 49.11°C, 48.51°C, 47.12°C, 43.32°C, 43.33°C, 43.22°C, 43.3°C, 49.38°C, and 48.93°C respectively. At 8C discharge rate, the peak temperatures reach 85.36°C, 82.36°C, 81.37°C, 82.63°C, 64.23°C, 64.27°C, 64.31°C, 74.08°C, and 74.32°C. At time 0.2 hours during the 8C discharge, the temperatures stabilize at 61.55°C, 58.55°C, 54.14°C, 53.89°C, 51.38°C, 51.68°C, 51.37°C, 58.05°C, and 57.14°C respectively. From this, we observe that M-B4, M-B5, and M-B6 consistently exhibit the lowest peak temperatures across all discharge rates, indicating superior cooling efficiency.

Discharge rate has a strong significance, and voltage drop is more noticeable at higher discharge rates impacting all the tested settings. The impact of the cooling method is equally relevant since a better way of cooling will contribute to stabilizing of voltage due to minimized thermal decay.

From observing the voltage data across various models at different discharge rates, we can analyze the performance of each configuration. At a 0.5C discharge rate, the voltages for Models M-A, M-B1, M-B2, M-B3, M-B4, M-B5, M-B6, M-C, and M-D are recorded as 4.03V, 4.04V, 4.04V, 4.04V, 4.04V, 4.04V, 4.04V, 4.04V, and 4.04V, respectively. At 1C discharge, the voltages remain relatively stable, with values

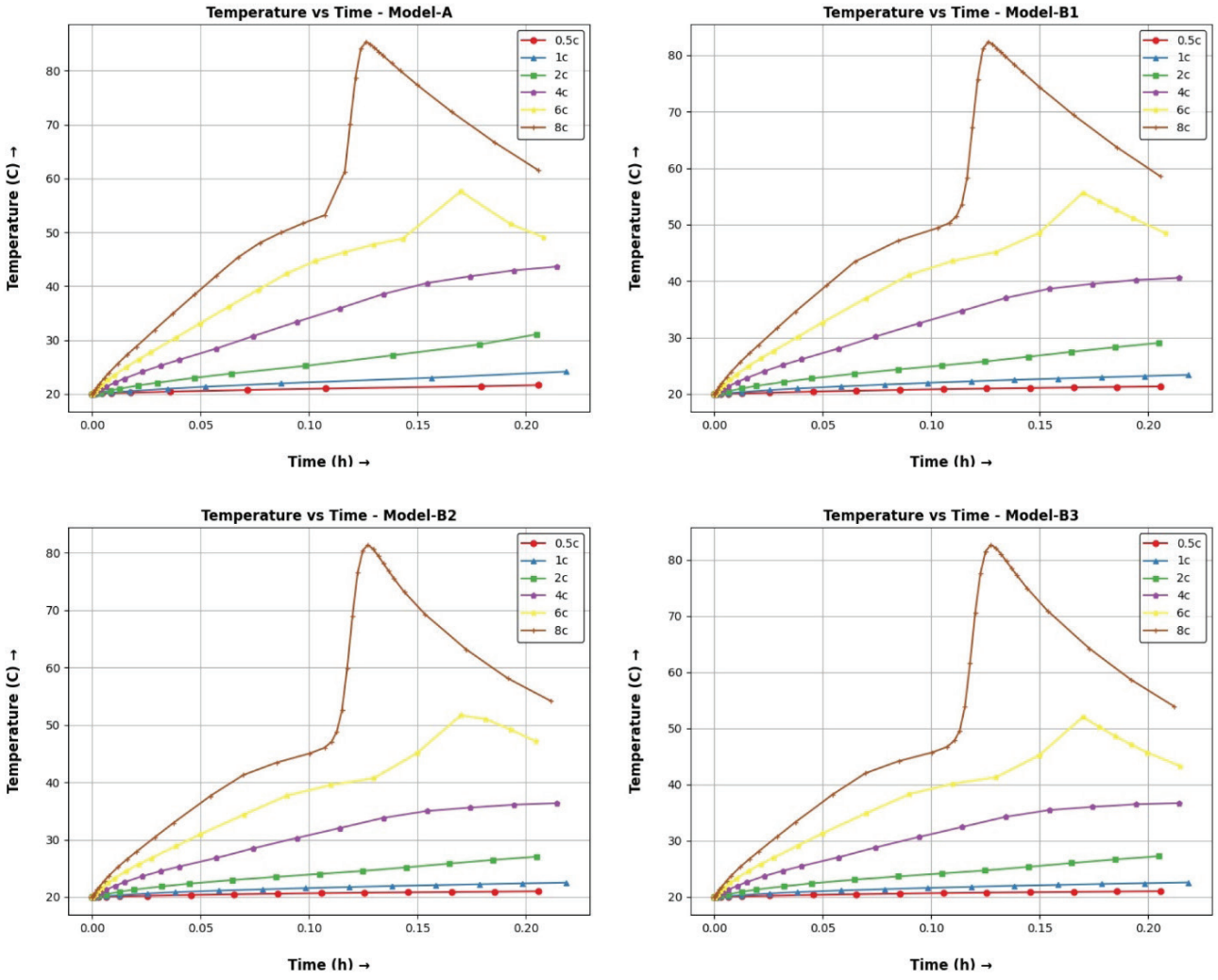

Figure 6(a). Peak Temperature Profiles of Model (M-A, M-B1, M-B2, and M-B3) Configuration Under Various Discharge Rates.

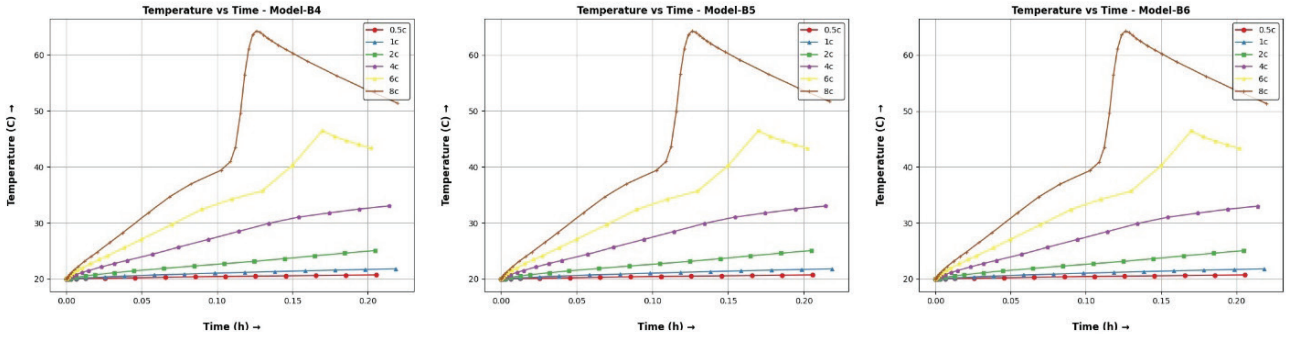

Figure 7(b). Peak Temperature Profiles of each Model (M-B4, M-B5, and M-B6) Configuration Under Various Discharge Rates.

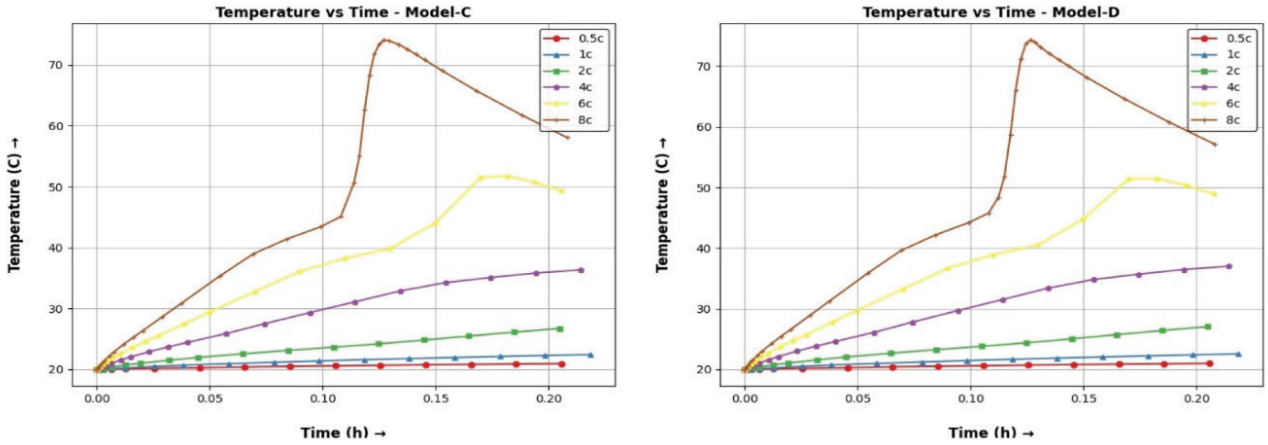

Figure 8(c). Peak Temperature Profiles of each Model (M-C and M-D) Configuration Under Various Discharge Rates.

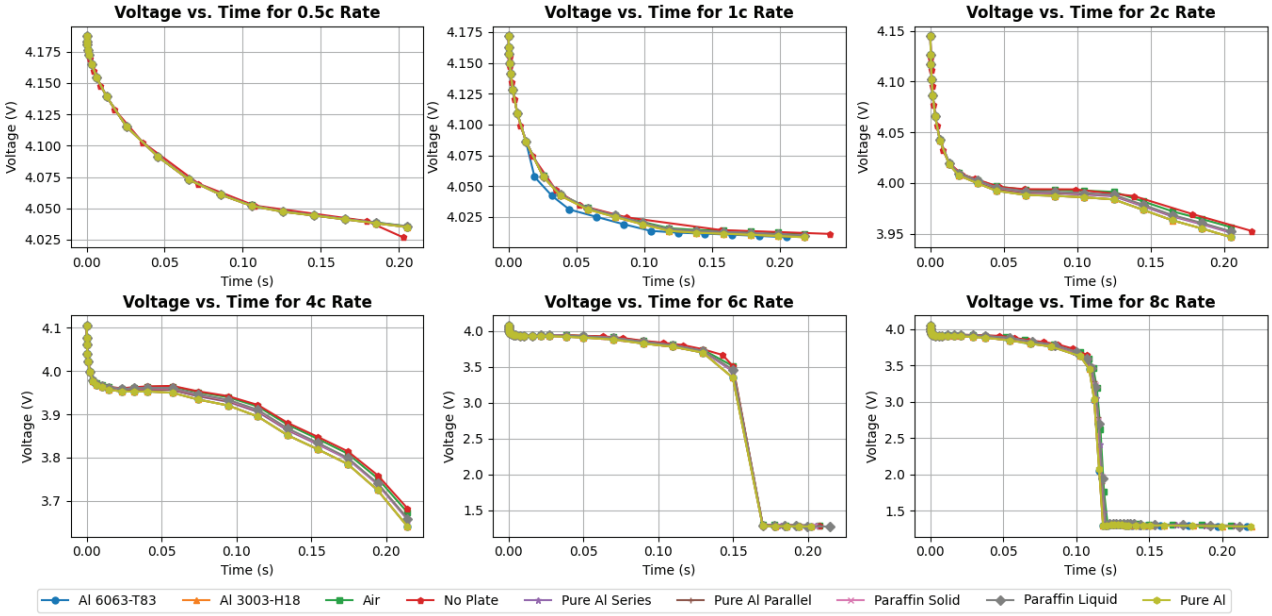

Figure 9. Voltage profiles per cell of Battery Pack Configurations Under Various Discharge Rates.

of 4.01V across most models, except for Model B4 through B6, which maintain the same voltage. When discharged at 2C, there is a slight drop in voltage, particularly for Models B1, B2, and B3, which exhibit voltages of 3.96V. The trend continues at 4C, where the voltages decrease further, with Model B4 reaching 3.64V, indicating a more significant impact of discharge rates on these models. At higher rates of 6C and 8C, voltages drop substantially, particularly for Model B6, which stabilizes at 1.27V at 6C and maintains 1.28V at 8C. This behavior suggests that Models B4, B5, and B6 consistently exhibit a higher capacity to retain voltage across varying discharge rates, indicating better performance and efficiency in voltage retention during operation.

Therefore, considering the thermal and electrical results, it is possible to state that M-B6 (Al 3003-H18) has the best results in temperature dissipation and voltage regulation at all the discharge current rates. A similar success is achieved by M-D (Aluminum in Parallel); it is optimal about the higher charge/discharge rates thus fitting well high-end functionalities.

The bar chart in figure 7 gives the direct comparison of peak temperatures at a given configuration at different discharge rates. This supports the observation made in Figure 4 and 5(a-c) with the help of Table 4 indicating that all techniques based on aluminum gives a lower peak temperature.

Thermal Distribution (Heat Profile)

The thermal distribution shown in Figure 7 is in the different battery pack configuration models M-A, M-B(1-6), M-C, and M-D at different discharge rates of 0.5C, 1C, 2C, 4C, 6C, and 8C. Each row represents a different cooling technique: The researched cooling types include no plate (M-A), air cooling (M-B1), paraffin solid and paraffin liquid cooling (M-B2 and M-B3), pure aluminum cooling (M-B4), aluminum variants (M-B5 and M-B6), and aluminum configurations in series and parallel (M-C and M-D).

The thermal maps reveal that M-A tends to exhibit a high degree of temperature variations, especially at a higher rate of discharge, which proves that the thermal regulation of this model is inadequate. The cooling techniques that use

Table 4. Comparison of Cooling Techniques for Battery Cells at Various Discharge Rates

Configuration	Parameter	0.5C	1C	2C	4C	6C	8C
Model A	Voltage at 0.2h (V)	4.03	4.01	3.96	3.68	1.29	1.29
	Temperature at 0.2h (°C)	21.64	24.15	31.08	43.64	49.11	61.55
	Peak Temperature Recorded (°C)	21.64	24.15	31.08	43.64	57.6	85.36
Model B1 (Air)	Voltage at 0.2h (V)	4.04	4.01	3.96	3.67	1.29	1.29
	Temperature at 0.2h (°C)	21.34	23.37	29.04	40.57	48.51	58.55
	Peak Temperature Recorded (°C)	21.34	23.37	29.04	40.57	55.66	82.36
Model B2 (Paraffin Solid)	Voltage at 0.2h (V)	4.04	4.01	3.95	3.66	1.28	1.29
	Temperature at 0.2h (°C)	20.99	22.51	27.02	36.35	47.12	54.14
	Peak Temperature Recorded (°C)	20.99	22.51	27.02	36.35	51.62	81.37
Model B3 (Paraffin Liquid)	Voltage at 0.2h (V)	4.04	4.01	3.95	3.66	1.28	1.29
	Temperature at 0.2h (°C)	21.02	22.59	27.25	36.72	43.32	53.89
	Peak Temperature Recorded (°C)	21.02	22.59	27.25	36.73	52.63	82.63
Model B4 (Aluminum)	Voltage at 0.2h (V)	4.04	4.01	3.95	3.64	1.27	1.28
	Temperature at 0.2h (°C)	20.7	21.82	25.07	33.02	43.33	51.38
	Peak Temperature Recorded (°C)	20.7	21.82	25.07	33.02	46.45	64.23
Model B5 (Al 6063-T83)	Voltage at 0.2h (V)	4.04	4.01	3.95	3.64	1.27	1.28
	Temperature at 0.2h (°C)	20.7	21.82	25.07	33.02	43.32	51.68
	Peak Temperature Recorded (°C)	20.7	21.82	25.07	33.02	46.46	64.27
Model B6 (Al 3003-H18)	Voltage at 0.2h (V)	4.04	4.01	3.95	3.64	1.27	1.28
	Temperature at 0.2h (°C)	20.7	21.82	25.06	33.01	43.3	51.37
	Peak Temperature Recorded (°C)	20.7	21.81	25.06	33.01	46.45	64.31
Model C (Aluminum in series)	Voltage at 0.2h (V)	4.04	4.01	3.95	3.66	1.29	1.29
	Temperature at 0.2h (°C)	20.95	22.44	26.73	36.34	49.38	58.05
	Peak Temperature Recorded (°C)	20.95	22.44	26.73	36.34	51.73	74.08
Model D (Aluminum in parallel)	Voltage at 0.2h (V)	4.04	4.01	3.95	3.66	1.29	1.29
	Temperature at 0.2h (°C)	21	22.57	27.05	37.01	48.93	57.14
	Peak Temperature Recorded (°C)	21	22.57	27.05	37.01	51.49	74.32

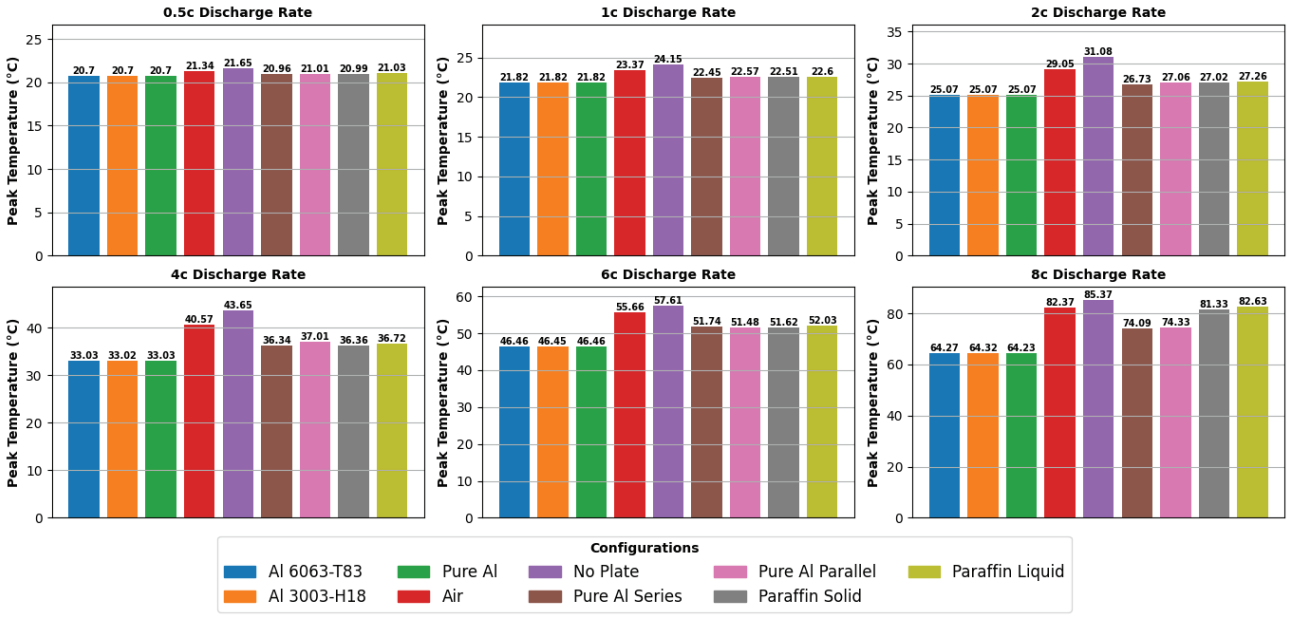

Figure 10. Comparison of Peak Temperatures for Battery Pack Configurations Across Different Discharge Rates.

air and paraffin (M-B1, M-B2 and M-B3) are also moderate effective at reducing the temperature, yet at high discharge rates; hot zones are still observed.

In the case of pure aluminum as well as the various aluminum derivatives (M-B4, M-B5, and M-B6), the heat dissipation is more evenly distributed and heat issues are not apparent even when operating at high discharge rates. The aluminum in the series and parallel (M-C and M-D) has the best thermal dissipation as it has the least isothermal changes across all rates of discharge. This figure for the most part conveys the information that aluminum-based cooling methods serve the best in heat removal and thermal regulation of battery packs.

Correlation Analysis for Various Discharge Rates

Correlation analysis proves to be an invaluable tool for both predictive accuracy and real-time application in industries like aerospace, where thermal management is critical. It offers valuable insights for material selection and performance prediction, helping to optimize thermal management techniques. The strength of the correlations between the models and materials across various discharge rates (0.5C to 8C) provides insights into how closely related the performance of different thermal management systems are under similar stress conditions.

The correlation matrices shown in Figure 8(a) to 8(c), depicts the correlation values of various measurements for different discharge rates (0. 5C, 1C, 2C, 4C, 6C, 8C). Each matrix is a 2 by 2 matrix, in which cells are the correlation coefficients between the two M-A and M-B (1-6), M-C and M-D. The numbers and color gradient alongside them represent the level of correlation, with numbers close to 1. While the closer to 1 means a positive direction, values

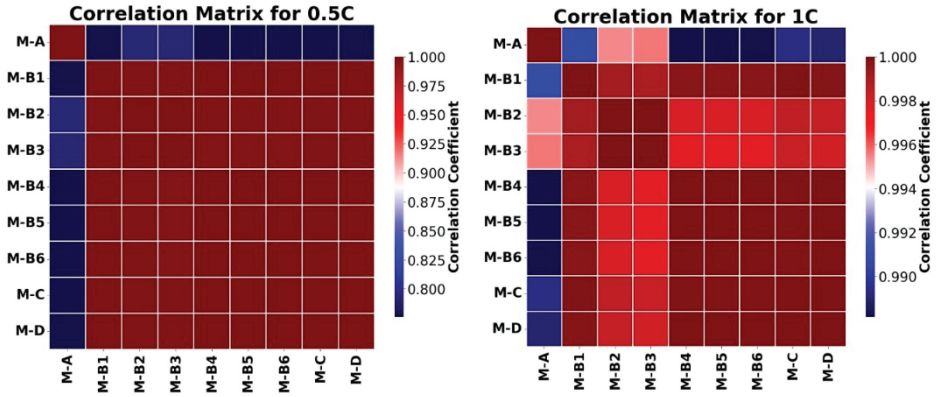

Figure 11(a). Correlation matrix of different models at 0.5C and 1C discharge rate.

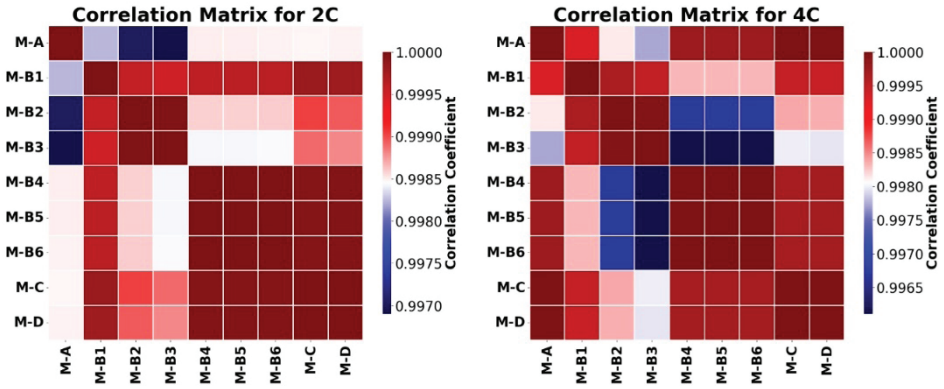

Figure 12(b). Correlation matrix of different models at 2C and 4C discharge rate.

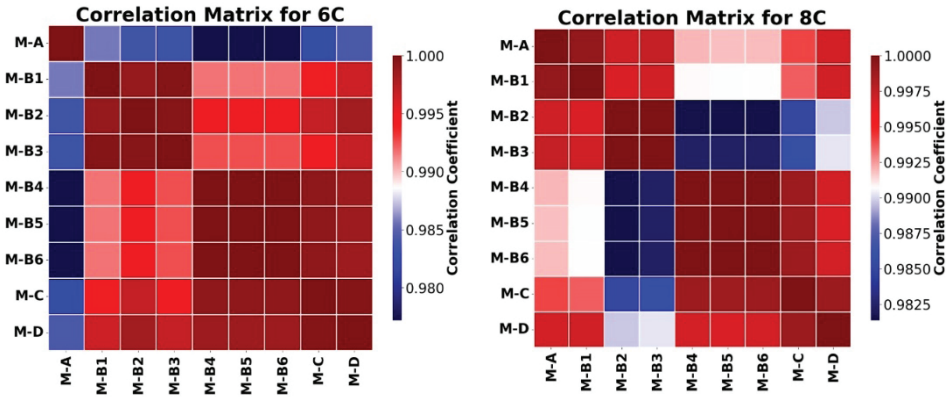

Figure 13(c). Correlation matrix of different models at 6C and 8C discharge rate.

closer to 0 mean negative direction and hence, 0 supports a strong positive direction. The correlation between these is -1 implying a negative correlation where values often give 0 it implies that there is no correlation.

Red represents strong positive correlations (closer to +1): Shows that one measurement has variation in direct proportion with the other. Blue represents strong negative correlations (closer to -1): Expresses that if the first variable is large, the second one is least and vice versa. No Correlation (close to 0): Used when there is no correlation between the measurements. At the 0.

In smaller aircraft like Piper, Cessna, and Cirrus, efficient thermal management is crucial for optimizing battery systems and overall performance. The correlation analysis reveals that aluminum and its alloys (M-B4, M-B5, M-B6, M-C, M-D) exhibit high consistency in thermal conductivity across all discharge rates, making them ideal for lightweight aircraft where minimizing heat buildup is essential. Paraffin-based Phase Change Materials (M-B2, M-B3) also show strong reliability, offering excellent thermal storage capabilities. For these aircraft, combining highly conductive materials like aluminum with PCMs could significantly improve cooling efficiency, ensuring stable performance, and extending the lifespan of energy systems in compact, high-demand environments. These insights align with current advancements in lightweight, efficient thermal management technologies used in modern aviation, potentially enhancing safety and energy efficiency in smaller aircraft systems.

Discharge rate of 0.5C, the results of the correlation matrix reveal that the models have different levels of positive correlation. It is also observed that there is moderate positive relationship between Model A (M-A) and other models wherein the weakest association was detected and the lowest with Model M-B2 at 0.7929. The models of aluminum and its alloys (M-B4, M-B5, M-B6, M-C, M-D) are very closely related with each other approaches the maximum value 1.0. This can be interpreted to mean that the thermal and electrical characteristics of these models are quite close when it comes to this given discharge rate.

Concerning the 1C discharge rates, the correlation coefficients trend is characterized by the increase of the figures, which shows the growing dependence of the models. These respective correlations range from being very strongly positively related as M-A with M-B1 at 0.9908. The models based on aluminum (M-B4, M-B5, M-B6, M-C, M-D) again and again depict close correlation, in some cases even arriving at

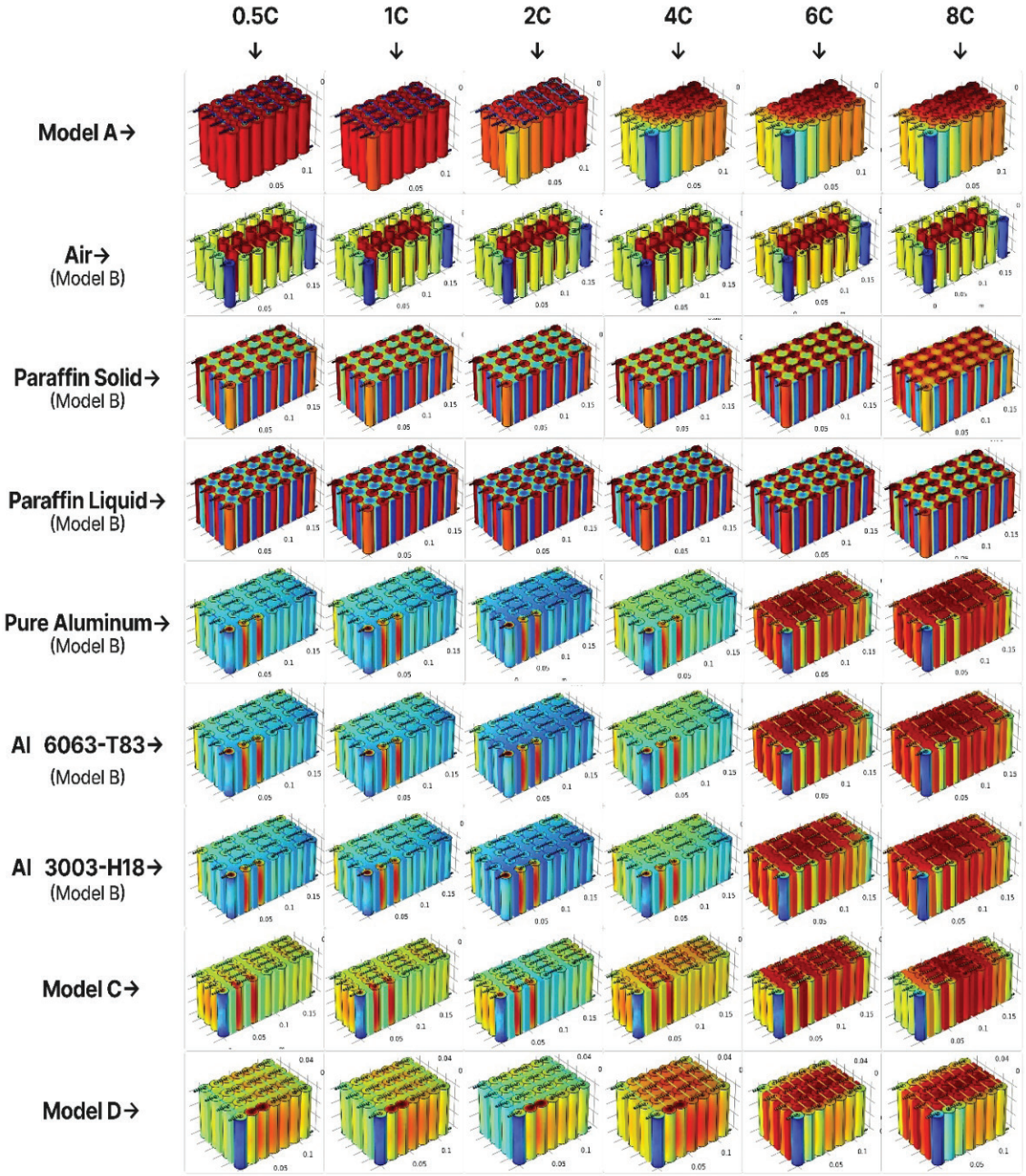

Figure 14. Thermal distribution in battery pack models A, B, C, and D across various discharge rates

the level of 0.999. Such a high correlation between the two models implies that the models' response to the thermal stresses is similar at this higher discharge rate.

At a 2C discharge rate, the correlation coefficients between the models are also considered to be high. This indicates that, Model A (M-A) has positive relationship with other models particularly Model B1 (M-B1) at 0.9982. All the models with paraffin and aluminum (M-B2, M-B3, M-B4, M-B5, M-B6, M-C, M-D) have the similar and high correlation coefficients, which gives evidence that the efficiency of the thermal management stratagem planning with the increased discharge condition is also satisfactory.

The same is also true when the discharge rate has been raised to 4C; the correlation matrix shows that M-A correlates with other models like M-B1 with an indication of 0.9993. The aluminum and its alloy models (M-B4, M-B5, M-B6, M-C, M-D) almost have 1:1 correlation coefficient, which depicts that these model's behavior is quite predictable and almost similar under this higher discharge stress.

Further, at the 6C discharge rate the association between different models reveal insignificant decline particularly between the M-A model and the others and the lowest value was recorded with M-B1 model as 0.9857. Nevertheless, considering their results under this discharge

rate, it is evident that the correlations in the thermal and electrical properties of the aluminum-based models (M-B4, M-B5, M-B6, M-C and M-D) are still very high and therefore; a strong positive relationship is still evident.

The correlation matrix shows very high correlation for most of the models for the level contributing to the highest discharge rate of 8C. M-A has a correlation coefficient of 0.9993 with M-B1. The same situation can be observed with aluminum and alloy models M-B4, M-B5, M-B6, M-B, M-D, with near-perfect coefficients which remained stable and prove the efficiency of the corresponding thermal management schemes at the maximum tested discharge rate as well.

M-A, Correlations range from 0.7759 to 0.9993 were reported. A striking feature of M-B1 is demonstrated to have very higher correlation coefficients with the other models that exceeds 0.990. M-B2 correlates almost perfectly with another aluminum-based model which shows that its performance is almost similar. M-B3 resembles M-B2 in terms of very high correlation. This study found out that M-B4 has a high correlation with other aluminum models in most models established constantly high correlations.

Frequently, the M-B5 correlation coefficients approach 1.0, indicating predictable performance. M-B6 is generally very high affinity with other models especially the aluminum-based models. Both M-C have a high correlation with other aluminum models particularly when the discharge rates are high. The values for M-D lay near one, meaning good performance and similarity between the model and other models.

CONCLUSION

Among all the cooling techniques, aluminum-based heat spreaders demonstrated superior thermal performance, with Al 3003-H18 showing the most effective results. At an 8C discharge rate, this model achieved a maximum temperature of 57.22°C, outperforming air cooling (82.62°C) and standard aluminum (64.23°C). Also, Al heat spreaders enhanced voltage regulation depending on the discharge current. For instance, that voltage drop for Al 3003-H18 was small, that retained 4.04V, 4.01V, 3.95V, 3.64V, and 1.27V at discharge rates from 0.5C to 8C, which pointed to the decreased thermal induced degradation. The positive correlation values of above all aluminum-based models briefed that they are showing consistent results and are very reliable when tested under different thermal conditions which confirm their use for aviation.

Air cooling, being easy and cheap, proved to have a low efficiency and further declined at high discharge rates (82.36°C) at 8C. This makes it less suitable for high-performance operations such as aerodynamics, thermals and other critical aviation uses. Paraffin solid and liquid (Phase Change Materials) provided moderate enhancements over passive air cooling at the same time. However, their peak temperatures at 8C (54.14°C and 53.89°C) were higher than the aluminum-based methods; thus, it can be deduced that the proposed techniques are more suitable for moderate thermal management but not at very high stresses.

Aluminum, especially Al 3003-H18, proved to be the best material for effective heat dissipation and maintaining uniform temperature distribution. The quantitative results, maintaining steady-state temperatures at 0.2 hours, 20.7°C, 21.82°C, 25.06°C, 33.01°C, 43.3°C, and 51.37°C at discharge rates from 0.5C to 8C, highlight aluminum's superior thermal conductivity and stability. The quantitative results, such as, coupled with minimal voltage drops, highlight aluminum's high thermal conductivity and stability. This makes it an ideal choice for high-performance and safety-critical applications in aviation.

Thus, assessment of this study's findings offers considerable value for the realization and monetization of effective thermal management systems in airborne applications. The obtained results indicate that the use of the aluminum-based cooling has a higher cooling effectiveness and therefore integrating the right kind of cooling into battery management systems will expand the safety, efficiency, and service time of lithium-ion batteries. As it could be observed from the aircraft manufacturers and operators' point of view, the described cooling techniques may lead to the improvement and durability of battery systems meeting the current load levels and operating conditions of modern aviation.

NOMENCLATURE

General Parameters

SOC	State of Charge
T	Temperature
t	Time (s)
x	Spatial coordinate (m)
r	Radial coordinate in spherical (m)
ρ	Density (kg/m^3)
c_p	Specific heat capacity at constant pressure (J/kg·K)
k	Thermal conductivity (W/m·K)
μ	Velocity vector (m/s)
τ	Characteristic time (s)

Electrical and Electrochemical Parameters

E_{cell}	Cell voltage (V)
$E_{OCV\,(SOC,T)}$	Open Circuit Voltage (V)
η_{IR}	Overpotential due to internal resistance (V)
η_{act}	Activation overpotential (V)
I_{cell}	Current through the cell (A)
I_{1C}	Current corresponding to a 1C rate (A)
$Q_{cell,0}$	Nominal capacity of the battery cell (Ah)

Thermal Parameters

Q_h	Total heat generation within the cell (W/m^3)
Q_{mix}	Heat generation due to mixing or diffusion (W/m^3)
$E_{OCV,therm}$	Thermal component of the open circuit voltage (V)

$E_{OCV,ref}$	Reference OCV at a reference temperature (V)
T_{ref}	Reference temperature (C)

Other Symbols

∇	Nabla operator (vector differential operator)
$\cdot$	Dot product
Ω	Domain of integration
d_{vol}	Differential volume element
k_s	Shell's thermal conductivity (W/m·K)
h_{nat}	Natural convective heat transfer coefficient of air (W/m²·K)
T_s	Temperature of the shell (K)
T_a	Ambient temperature (K)
n	Direction normal (wall-normal direction)

AUTHORSHIP CONTRIBUTIONS

Authors equally contributed to this work.

DATA AVAILABILITY STATEMENT

The authors confirm that the data that supports the findings of this study are available within the article. Raw data that support the finding of this study are available from the corresponding author, upon reasonable request.

CONFLICT OF INTEREST

The author declared no potential conflicts of interest with respect to the research, authorship, and/or publication of this article.

ETHICS

There are no ethical issues with the publication of this manuscript.

STATEMENT ON THE USE OF ARTIFICIAL INTELLIGENCE

Artificial intelligence was not used in the preparation of the article.

REFERENCES

[1] Lithium-ion aircraft batteries as a smoke/fire risk. SKYbrary Aviation Safety. Jul 24, 2024. Available at: https://skybrary.aero/articles/lithium-ion-aircraft-batteries-smokefire-risk Accessed on Sep 04, 2025

[2] Lithium-ion batteries for aerospace applications. Nanografi Nano Technology. Available at: https://nanografi.com/blog/lithiumion-batteries-for-aerospace-applications/ Accessed on Sep 04, 2025

[3] Special conditions: Boeing Model 777-200, -300, and -300ER series airplanes; rechargeable lithium-ion batteries and battery systems. Fed Regist. Dec 19, 2013. Available at: https://www.federalregister.gov/documents/2013/12/19/2013-30232/special-conditions-boeing-model-777-200--300-and--300er-series-airplanes-rechargeable-lithium-ion Accessed on Sep 04, 2025

[4] Lithium-ion batteries. KADEX Aero Supply. Dec 23, 2021. Available at: https://kadexaero.com/product-details/advanced-lithium-ion-main-batteries/ Accessed on Sep 04, 2025

[5] Gill 7242-16 LT series 24-volt/16Ah super capacity sealed lead acid aircraft battery. SkyGeek. Available at: https://skygeek.com/gill-7242-16-aircraft-battery.html Accessed on Sep 04, 2025

[6] Gill 7243-16 LT sealed lead acid battery. Aircraft Spruce. Available at: https://www.aircraftspruce.com/catalog/elpages/gill7243battery11-12210.php Accessed on Sep 04, 2025

[7] COMSOL Inc. COMSOL Multiphysics reference manual, version 5.6. Burlington: COMSOL Inc.; 2020. Available at: file:///C:/Users/mmrun/Downloads/COMSOL_ReferenceManual.pdf Accessed on Sep 04, 2025

[8] Liu S, Zhang G, Wang CY. Challenges and innovations of lithium-ion battery thermal management under extreme conditions: a review. ASME J Heat Mass Transfer 2023;145:082301. [CrossRef]

[9] Figueiras I, Coutinho M, Afonso F, Suleman A. On the study of thermal-propulsive systems for regional aircraft. Aerospace 2023;10:113. [CrossRef]

[10] Coutinho M, Afonso F, Souza A, Bento D, Gandolfi R, Barbosa FR, et al. A study on thermal management systems for hybrid–electric aircraft. Aerospace 2023;10:745. [CrossRef]

[11] Capron O, Samba A, Omar N, Gualous H, Bossche P, Mierlo J. Large and high-power cylindrical batteries: analysis of the battery packs temperature distributions using COMSOL Multiphysics and MATLAB simulation softwares. 2014. Available from: https://www.semanticscholar.org/paper/Large-and-High-Power-Cylindrical-Batteries-Analysis-Capron-Samba/7a05ff0820328120ae9cb6500aac7fc6ec6a966d Accessed on Sep 04, 2025

[12] Shetty DD, Venugopal V, PR, Zuber M, Badruddin IA, Kini C. Computational flow analysis of different streamline cooling plates for thermal management of lithium-ion battery. Cogent Eng 2022;9:2048996. [CrossRef]

[13] Zhu Y, Li K, Kang E, Quan T, Sun T, Luo J, et al. Simulation investigation on thermal characteristics of thermal battery activation process based on COMSOL. Crystals 2023;13:641. [CrossRef]

[14] Zhao Y, Chen J, He W. Design and performance evaluation of liquid-cooled heat dissipation structure for lithium battery module. Processes 2023;11:1769. [CrossRef]

[15] Dunning J, Mackin T, Rozsnyo R. Heat generation modeling of a lithium battery: from the cell, to the pack on COMSOL Multiphysics. 2015. Available from: https://

www.semanticscholar.org/paper/Heat-Generation-Modeling-of-a-Lithium-Battery%3A-from-Dunning-Mackin/fc0ff5f40f7fc71b69fc906dec8ea2295b76e99a Accessed on Sep 04, 2025.

[16] Sun J, Dan D, Wei M, Cai S, Zhao Y, Wright E. Pack-level modeling and thermal analysis of a battery thermal management system with phase change materials and liquid cooling. Energies 2023;16:5815. [CrossRef]

[17] Satheesh VK, et al. Enhancement in air-cooling of lithium-ion battery packs using tapered airflow duct. J Therm Eng 2024;10:375−385. [CrossRef]

[18] Gharde PR, Havaldar SN. Numerical investigation of an amalgamation of two-phase change materials thermal energy storage system. J Therm Eng 2024;10:263−272. [CrossRef]

[19] Gungor S, Gocmen S, Cetkin E. A review on battery thermal management strategies in lithium-ion and post-lithium batteries for electric vehicles. J Therm Eng 2023;9:1078−1099. [CrossRef]

[20] Palmieri B, Cilento F, Siviello C, Bertocchi F, Giordano M, Martone A. Mitigation of heat propagation in a battery pack by interstitial graphite nanoplatelet layer: coupled electrochemical-heat transfer model. J Compos Sci 2022;6:296. [CrossRef]

[21] COMSOL Inc. Introduction to battery design module. COMSOL Multiphysics Documentation. 2021. Available at: https://doc.comsol.com/6.1/doc/com.comsol.help.battery/IntroductionToBatteryDesignModule.pdf Accessed on Sep 04, 2025.